doi.org/10.36721/PJPS.2024.37.2.REG.275-289.1

Exploring *Zingiber officinale* bioactive compounds for inhibitory effects on *Streptococcus pneumoniae* capsular polysaccharide biosynthesis proteins: *In silico* study

Muhammad Bilal Azmi[1]*, Muhammad Yahya Noori[2], Syed Danish Haseen Ahmed[1], Bader Saud Alotaibi[3], Sadaf Naeem[4], Mohsin Kazi[5], Muhammad Islam[6] and Abdul Wadood[6]

[1]Computational Biochemistry Research Laboratory, Department of Biochemistry, Dow Medical College, Dow University of Health Sciences, Karachi, Pakistan
[2]Department of Pathology, Dow Medical College, Dow University of Health Sciences, Karachi, Pakistan
[3]Department of Clinical Laboratory Sciences, College of Applied Medical Sciences, Al-Quwayiyah, Shaqra University, Riyadh, Saudi Arabia
[4]Department of Biochemistry, University of Karachi, Karachi, Pakistan
[5]Department of Pharmaceutics, College of Pharmacy, King Saud University, Riyadh, Saudi Arabia
[6]Department of Biochemistry, Abdul Wali Khan University, Mardan, Pakistan

Abstract: The capsule is a major virulence factor for *Streptococcus pneumoniae* which causes global morbidity and mortality. It is already known that there are few conserved genes in the capsular biosynthesis pathway, which are common among all known serotypes, called *CpsA*, *CpsB*, *CpsC* and *CpsD*. Inhibiting capsular synthesis can render *S. pneumoniae* defenseless and vulnerable to phagocytosis. The Inhibitory potential of active *Zingiber officinale* compounds was investigated against the 3D (3-dimensional) structural products of *Cps* genes using *in silico* techniques. A 3D compound repository was created and screened for drug-likeness and the qualified compounds were used for molecular docking and dynamic simulation-based experiments using gallic acid for outcome comparison. Cavity-based docking revealed five different cavities in the CpsA, CpsB and CpsD proteins, with gallic acid and selected compounds of *Zingiber* in a binding affinity range of -6.8 to -8.8 kcal/mol. Gingerenone A, gingerenone B, isogingerenone B and gingerenone C showed the highest binding affinities for CpsA, CpsB and CpsD, respectively. Through the Molegro Virtual Docker re-docking strategy, the highest binding energies (-126.5 kcal/mol) were computed for CpsB with gingerenone A and CpsD with gingerenone B. These findings suggest that gingerenone A, B and C are potential inhibitors of *S. pneumoniae*-conserved capsule-synthesizing proteins.

Keywords: Gallic acid, gingerenone, polysaccharide capsule, *Streptococcus pneumonia, Zingiber officinale*.

INTRODUCTION

Streptococcus pneumoniae (also known as "*pneumococcus"*) is responsible for millions of deaths worldwide (Oligbu *et al.,* 2019). These bacteria are encapsulated gram-positive cocci, which commonly cause pneumonia, sepsis, meningitis and middle ear infections (Jayaraman *et al.,* 2019). *S. Pneumoniae* contains a variety of virulence factors which enable it to evade host immune systems and enhance adhesion, tissue invasion and other virulence-related behaviors (Subramanian *et al.,* 2019). Although vaccines are available;, the presence of nearly 100 pneumococcal serotypes, due to different capsular structures makes the control of this organism challenging (Gonzales-Siles *et al*., 2019).

The *pneumococcal* capsule is a major virulence factor of *S. pneumoniae* (Paton and Trappetti, 2019) is composed of a polysaccharide layer that surrounds the bacterium and acts as a barrier to prevent recognition and phagocytosis by the host immune cells. It also helps in bacterial adherence to host tissues and resists antimicrobials (Gonzales-Siles *et al.,* 2019; Geno *et al.,* 2015). Genes for capsule biosynthesis are present at a locus found between two genes *dexB* and *aliA*. This locus can vary from 10 kb to 37 kb and may consist of several genes. Four of these genes, *cpsA (wzg), cpsB (wzh), cpsC (wzd) and cpsD (wze),* have been reported to be conserved across all serotypes (Gonzales-Siles *et al*., 2019).

Natural products have been shown to have potential in the treatment of respiratory infections. Many of these could be caused by *S. pneumoniae* (Oriola and Oyedeji, 2022; Timalsina *et al.,* 2021). In addition to this natural products have been found to have antimicrobial activity against *pneumococcus* (Elmaidomy *et al.,* 2022). Since there is growing evidence of pneumocccal resistance to antibiotics (Aliberti *et al.,* 2019) and reports of vaccine escape, (Croucher *et al.,* 2014), there is a need for new drug development.

In this project, *in silico* techniques were used to investigate the inhibitory potential of bioactive compounds from *Zingiber officinale* against 3D structural products of conserved genes of capsule-synthesizing proteins from *S. pnuemoniae*. Commonly known as ginger, *Zingiber officinale* has been utilized in traditional

**Corresponding author:* e-mail: bilal.azmi@duhs.edu.pk

medicine for thousands of years (Mao *et al.,* 2019; Ozkur *et al.,* 2022) and its extracts have been reported to have inhibitory activity on the growth of *pneumococci* and other pathogenic bacteria (AlSheikh *et al.,* 2020; Oyinlola *et al.,* 2022). Therefore, in this study, the active *ginger* compounds were tested against 3D structural products of conserved genes of capsule-synthesizing proteins from *S. pneumoniae*.

MATERIALS AND METHODS

Retrieval of bacterial gene sequences

After a thorough literature search, the conserved capsular polysaccharide (CPS) biosynthesis gene targets were obtained from the available pneumococcal serotypes. The genes *cpsA, cpsB, cpsC and cpsD* of *S. pneumoniae* were included in the present investigation to explore the inhibitory potential of the bioactive compounds from *Zingiber officinale* in inhibiting the products of the conserved CPS biosynthesis genes (AlSheikh *et al.,* 2020; Gonzales-Siles *et al*., 2019; Zhang *et al.,* 2021). The conserved gene sequences (CPS biosynthesis genes *cpsA, cpsB, cpsC and cpsD*) of *S. pneumoniae* were retrieved from the National Center for Biotechnology Information (NCBI) and UniProt Knowledge Base (UniProtKB) databases (Rangwala *et al.,* 2021; Wang *et al.,* 2021). Gene sequences for CPS biosynthesis proteins were validated using manual annotation, literature extraction and computational analysis, with records cross-validated and saved with NCBI accession number FASTA format and gene identifier (Rangwala *et al.,* 2021).

Preparation of protein targets

Protein basic local alignment search tool (pBLAST) analysis was performed to generate alignments between the extracted protein sequences of CPS biosynthesis genes (*cpsA, cpsB, cpsC and cpsD*) of *S. pneumoniae* (as a "query") and protein sequences within a database record (as "subject" sequences) (Shah *et al.,* 2019). The strategy chosen to search the respective set for the Protein Basic Local Alignment Search Tool (pBLAST) was set with 'Protein Data Bank (PDB)' reported 3D structures (Shah *et al.,* 2019). The study selected the canonical coding gene sequences and obtained 3D structures, active site details and ligand interactions from the Protein Data Bank (PDB) (Goodsell *et al*., 2020). In cases where 3D structural information was lacking, homology modeling via MODELLER was conducted (Webb and Sali, 2021).

Validation and energy minimization of 3D protein models

Validation of the 3D model was carried out by PROCHECK stereochemical examination using the Ramachandran plot (https://prosa.services.came.sbg.ac.at/prosa.php). The protein 3D model was confirmed free of ligands and heteroatoms and UCSF Chimera was used for structure cleaning and refining, allowing interactive visualization of the resulting structure (Pettersen *et al.,* 2021). The DeepView/Swiss-PdbViewer tool was utilized for energy minimization of the modeled PDB structure files of CPS biosynthesis proteins from *S. pneumoniae* (Guex *et al.,* 2009).

Preparation of 3D natural products library

The NCBI PubChem database (Kim *et al.,* 2019) was used for the retrieval of natural compounds from *Zingiber officinale*. Initially, the retrieved 3D structures of the compounds were stored in the Structure-Data File (SDF) format and saved in the local repository of the system. The obtained 2D compound format was converted into a 3D PDB format using the Open Babel tool with the simultaneous addition of coordinates, hydrogen and neutral pH status (Yoshikawa and Hutchison, 2019). Energy minimization of the ligand library was performed using the PyRx docking tool (Dallakyan and Olson, 2015). Furthermore, the ligand library was prepared by adding Gastieger charges to compounds and torsion angles were applied by rotating all rotatable bonds using the AutoDock tool. Finally, the optimized compound library was saved in both PDB and PDBQT formats for further virtual screening (Dallakyan and Olson, 2015; Nguyen *et al.,* 2020).

Compound drug-likeness evaluation and property assessment

The evaluation of the properties of the compounds in terms of drug-likeness was analyzed for cross-validation of the compound as a suitable therapeutic candidate. Lipinski's Rule of Five was used to evaluate the drug-likeness of the compounds (Chen *et al.,* 2020). Following the assessment, only 3D compounds of *Zingiber officinale* that passed all five physicochemical properties of Lipinski's rule of five were chosen, as any single violation was considered an elimination aspect or treated as a "fail". The drug-likeness properties were further computed and validated using OSIRIS Property Explorer (https://www.organic-chemistry.org/prog/peo/).

Identification of druggable binding cavities in target genes

To detect protein-binding druggable cavities, cavity-binding (CB) docking (Liu *et al.,* 2022) was used to generate consensus interaction cavities present in the proteins encoded by CPS biosynthesis genes. Cavity detection (CB)-guided blind docking explored the binding cavities of the homology model through an automatic protein-ligand docking approach that identifies the binding cavities and sites. CB Dock compared cavities and ranked them through a method called 'CurPocket' with state-of-the-art protein-ligand binding site prediction methods using the benchmark set of COACH (Liu *et al.,* 2020) as a prediction method. CB Dock also calculates the center and size of the docking box of the putative cavity as key parameters of the process using a novel curvature-based cavity detection approach. This method carefully optimizes and achieves a ~70% success rate for the top-ranking poses whose root mean square deviation (RMSD) was within 2 Å from the X-ray pose (Liu *et al.,* 2022). The 3D structure of gallic acid, a standardized phenolic derivative, was used for outcome comparison, as

it possesses bactericidal activity by inhibiting CPS biosynthesis in other hyper-virulent gram-negative opportunistic pathogens (Lin *et al.,* 2022). Initially, to compare the successful cavity-based docking interaction, the main purpose was to recruit Gallic acid as a ligand molecule and its 3D structure was downloaded from the PubChem compound library (Kim *et al.,* 2019). The protocol identifies druggable protein cavities using a cavity-binding docking approach. 3D protein models of capsular polysaccharide biosynthesis genes are evaluated with ligands to identify potential cavities. The template-independent cavity detection method identifies five cavities, with each ranked based on CurPocket ID, cavity volume and size (Liu *et al.,* 2022). The study selected three top graded cavities for blind docking with *Zingiber officinale* bioactive compounds, resulting in five best binding affinities. The highly ranked cavity was used to investigate amino acid, protein-ligand interactions, bond nature and hydrogen bond formation. The strongest binding affinity was validated for accurate structural prediction using Discovery Studio Visualizer (Gao and Huang, 2011).

Molecular dynamic (MD) simulation of the top-ranked protein-ligand complex

To investigate and explore the ligand stability in the protein crystal structure, molecular dynamic simulation was carried out using AMBER 22 (Salomon-Ferrer *et al.,* 2013; Wadood *et al.,* 2022). The protein-ligand complex topology parameters were adjusted in AMBER leap. Amber force fields FF14SB for protein, with Gaff2 for ligand, were used to describe the protein-ligand complex. A TIP3P water module containing 8Å cubic boxes was used to solvate the protein-ligand complexes. The total charge on the protein-ligand complex and solvated system was neutralized in leap by adding (Na^+) or (Cl^-). Before going for MD simulation, the neutralized system was subjected to two-step minimization of 500 steps descent steepest and an additional 500 conjugate minimization to properly optimize and relax the system. Langevin dynamics algorithms were used to supervise thermal fluctuation and SHAKE algorithms were used to constrain bonds involving hydrogen atoms. The optimized system was gradually heated to a temperature of 0 K to 300 K throughout 100 ps under constant volume (NVT) and pressure (NPT) conditions. The system was then further equilibrated at 300 K for 100 ps (pico-second) to reach a thermodynamic equilibrium state. The particle mesh Ewald (PME) method was utilized to handle long-range electrostatic interactions, while a cutoff of 10 Å was utilized for nonbonded interactions. After equilibration, the system was subjected to a 50 ns (nanoseconds) MD simulation on PMEMD (Particle Mesh Ewald Molecular Dynamics) CUDA version on a GPU. The trajectories of the MD simulations were analyzed with the CPPTARJ module of AMBER22 (Wadood *et al.,* 2022). Visualization and graphical representation of trajectory analysis were carried out using PyMOL and OriginPro.

Re-docking through the molegro virtual docker (MVD) platform

As a validation step, only those proteins were selected that have major structural coverage with prominent crystallographic or NMR-based structures available in the PDB. Afterward, all the screened compounds (ligands) exhibiting drug-likeness properties were re-docked with the selected protein structures through the Molegro Virtual Docker (MVD) tool (Bitencourt-Ferreira and de Azevedo, 2019). The approach utilized differential optimization and a user interface experience to achieve high-quality docking-based output, enhancing credibility in drug design processes. The ligand-protein molecules were prepared by adding charges, hydrogen and pliable torsions and their valences and hydrogen atoms were thoroughly examined.

Docking simulations involved ten runs, each ligand docking within the protein's active site, resulting in ten poses with MolDock scores, with the highest score used for selection and reporting (Bitencourt-Ferreira and de Azevedo, 2019). These highest MolDock score poses were recognized as the ones with the highest binding affinity, which could serve as effective inhibitors of CPS biosynthesis in *S. pneumoniae*. The amino acid interactions with ligands were individually examined through 2D ligand plots and 3D visualization analysis (Gao and Huang, 2011).

Ethical approval

Ethical review and approval were waived for this study by the Institutional Review Board of Dow University of Health Sciences, Karachi, Pakistan (Ref#IRB-2700/ DUHS/EXEMPTION/2022/1028, dated: 13th September, 2022) due to *in silico* analysis with no involvement of humans or animals.

RESULTS

Conserved capsular polysaccharide biosynthesis gene and protein targets

The NCBI database was used to download four capsular polysaccharide biosynthesis gene sequences for *S. pneumoniae*, with accession numbers CAI32719.1, WP_000565352.1, AEO88769.1 and WP_001142502.1 respectively. Among the four selected capsular proteins, *CpsA* had the highest number of amino acid residues, *i.e.,* 484. All other relevant details for these genes and proteins are mentioned in table 1.

During pBLAST analysis, three proteins were identified: CpsA, CpsB and CpsD, showing sequence alignment, query coverage and percent identity with other respective proteins present in the PDB repository (table 2). In particular, the highest (100%) structural alignment was observed in the CpsB protein of *S. pneumoniae*; therefore, for better interpretation and precision, completely adopted the PDB-based homology model '2WJD'.

Table 1: Details of the CPS of *S. pneumoniae* genes and proteins used in the present study

CPS Biosynthesis Protein	Gene	Protein	UniProt ID	NCBI Accession ID	Amino Acids	Molecular Weight	Total Atoms	Theoretical *pI*	Aliphatic Index	GRAVY
CpsA	*wzg*	Integral membrane regulatory protein Wzg	Q4K376	CAI32719.1	484	53871	7690	8.53	109.71	0.048
CpsB	*cpsB/wzh*	Tyrosine-protein phosphatase CpsB	Q9AHD4	WP_000565352.1	243	28131.3	3971	6.16	91.89	-0.424
CpsC	*wzd*	Capsular polysaccharide biosynthesis protein CpsC	G3GGW8	AEO88769.1	231	25615.89	3706	7.83	114.24	0.048
CpsD	*cpsD/wze*	Tyrosine-protein kinase CpsD	Q9AHD2	WP_001142502.1	227	24886.67	3552	8.96	97.93	-0.118

Table 2: Sequence alignment and protein-protein Basic Local Alignment (pBLAST) search of selected CPS biosynthesis proteins of *S. pneumoniae*

CPS Biosynthesis Protein	Description	Organism	Max Score	Total Score	Query Cover	E value	Identity (%)	Accession Length	Accession
CpsA	A widespread family of bacterial cell wall assembly proteins [*Streptococcus pneumoniae* D39]	*Streptococcus pneumoniae* D39	780	780	79%	0	99.74	398	2XXP_A
	A widespread family of bacterial cell wall assembly proteins [*Streptococcus pneumoniae* D39]	*Streptococcus pneumoniae* D39	777	777	79%	0	99.48	398	2XXQ_A
	LytR-Cps2a-Psr family protein with bound octaprenyl monophosphate lipid [*Streptococcus pneumoniae* D39]	*Streptococcus pneumoniae* D39	776	776	79%	0	99.74	397	4DE8_A
CpsB	Crystal structure of the tyrosine phosphatase Cps4B from *Steptococcus pneumoniae* TIGR4 [*Streptococcus pneumoniae*]	*Streptococcus pneumoniae*	501	501	100%	0	100	247	2WJD_A
	Crystal structures of YwqE from *Bacillus subtilis* and CpsB from *Streptococcus pneumoniae*, unique metal-dependent tyrosine phosphatases [*Streptococcus pneumoniae*]	*Streptococcus pneumoniae*	500	500	100%	0	100	251	3QY8_A
CpsD	Crystal structure of the chimerical protein CapA1B1 in complex with ADP-Mg [*Staphylococcus aureus*]	*Staphylococcus aureus*	112	112	88%	9E-30	36.59	269	4JLV_A
	crystal structure of the chimerical protein CapAB [*Staphylococcus aureus*]	*Staphylococcus aureus*	103	103	88%	4E-26	34.47	271	3BFV_A
	Crystal structure of the chimerical protein CapA2B2 [*Staphylococcus aureus*]	*Staphylococcus aureus*	103	103	88%	4E-26	34.47	269	4JMP_A
	crystal structure of the chimerical mutant CapABK55M protein [*Staphylococcus aureus*]	*Staphylococcus aureus*	100	100	88%	3E-25	33.98	271	2VED_A
	Crystal Structure of VpsO (VC0937) Kinase domain [*Vibrio cholerae*]	*Vibrio cholerae*	82.4	82.4	83%	2E-18	34.21	235	6U1Q_A
	Chain A, BceF [*Burkholderia cepacia*]	*Burkholderia cepacia*	80.9	80.9	87%	1E-17	31	271	6Z0P_A

Table 3: CB docking for the identification of protein-druggable pockets in the CpsA protein of *S. pneumonia*

Compound	Binding affinity (kcal/mol)	Cavity volume (Å3)	Center (x, y, z)	Docking size (x, y, z)	Contact Residues	Ligand Interactions	H-bond
Gallic acid	-6.4	4952	-8, 37, -22	26, 35, 35	GLY235 ILE236 ASP237 ARG247 SER248 ASP249 VAL250 ARG270 LEU316 ASN317 PHE318 PHE321 LEU361 VAL364 ARG365 ARG377 GLN381	GLY235 ILE236 VAL250 ARG 365 GLN 381	GLY235 ILE236 GLN 381
6-Gingerol	-7.2	4952	-8, 37, -22	24, 35, 35	VAL233 GLY235 ILE236 ASP237 THR238 VAL250 VAL314 LEU316 ASN317 PHE318 PHE321 MET324 LEU361 VAL364 ARG365 GLN381 VAL384 ILE385 ILE388 ILE412	ILE236 VAL250 VAL314 LEU316 PHE318	ILE236
6-Shagaol	-7.8	4952	-8, 37, -22	24, 35, 35	VAL233 GLY235 ILE236 ASP237 ASP249 VAL250 ARG270 VAL314 ARG315 LEU316 PHE318 PHE321 MET324 LEU361 VAL364 ARG365 ARG377 GLN381 ILE385 ILE412	VAL233 VAL250 VAL314 LEU316 MET324 VAL364 ARG365 ILE412	–
8-Gingerol	-6.4	4952	-8, 37, -22	24, 35, 35	PHE229 MET254 VAL256 ARG258 LYS261 ILE263 LEU389 LEU392 THR393 ALA397 LEU398 TYR401 ILE404 MET421 LEU424 VAL425 GLN428 TYR435	PHE229 VAL256 ILE263 LEU389 LEU392 ALA397 LEU398 ILE404 LEU424 GLN428 TYR435	GLN428 TYR435
10-Gingerol	-6.9	386	-4, 25, -41	26, 26, 26	VAL233 GLY235 ASP237 ASP249 VAL250 ARG270 LEU316 ASN317 PHE318 PHE321 LEU342 HIS343 LEU361 VAL364 ARG365 GLU366 TYR368 ARG377 GLN381 ILE385	ASP237 VAL250 ARG270 PHE318 PHE321 LEU361 VAL364 ARG365 TYR368 ARG377	ASP237 ARG270 TYR368 ARG377
Gingerenone A	-8.8	4952	-8, 37, -22	21, 35, 35	ILE231 VAL233 GLY235 ILE236 ASP237 ASP249 VAL250 MET254 ARG270 VAL314 LEU316 PHE318 PHE321 MET324 LEU361 VAL364 ARG365 ARG377 GLN381 ILE385 ILE388 LEU389 LEU392	VAL233 ASP249 VAL250 VAL314 LEU316 PHE321 VAL364 ARG365 ILE385 ILE388	ASP249
Gingerenone B	-8.6	4952	-8, 37, -22	28, 35, 35	ILE231 VAL233 GLY235 ILE236 ASP237 ASP249 VAL250 MET254 ARG270 VAL314 LEU316 PHE318 PHE321 MET324 LEU361 VAL364 ARG365 ARG377 GLN381 ILE385 LEU389 LEU392 ILE412	VAL233 VAL250 MET254 VAL314 LEU316 PHE321 MET324 VAL364 ARG365 ILE385 LEU389 ILE412	
Gingerenone C	-8.7	4952	-8, 37, -22	24, 35, 35	ILE231 VAL233 GLY235 ILE236 ASP237 THR238 VAL250 MET254 VAL314 LEU316 ASN317 PHE318 THR319 PHE321 MET324 LEU361 VAL364 VAL384 ILE385 ILE388 LEU389 LEU392 ILE412 THR414	VAL250 VAL314 LEU316 PHE321 VAL364 LEU392 ILE412	
Isogingerenone B	-8.3	4952	-8, 37, -22	27, 35, 35	ILE231 VAL233 GLY235 ILE236 ASP237 THR238 ASP249 VAL250 VAL314 LEU316 ASN317 PHE318 PHE321 MET324 LEU361 VAL364 ARG365 ILE385 ILE388 LEU389 LEU392 LEU408 ILE412	ILE236 VAL250 VAL314 LEU316 PHE318 PHE321 VAL364 LEU392 LEU408 ILE412	ILE236
Paradol	-6.3	386	-4, 25, -41	24, 24, 24	GLY235 ILE236 ASP237 ARG247 ASP249 VAL250 ARG270 LEU316 PHE318 PHE321 LEU361 VAL364 ARG365 TYR368 ARG377 GLN381	ASP237 ASP249 VAL250 ARG270 PHE318 PHE321 VAL364 ARG365 ARG377	
Zingerone	-5.6	4952	-8, 37, -22	26, 35, 35	PHE229 ILE231 MET254 VAL256 ARG258 ILE263 LEU389 THR393 LEU398 ASN423 LEU424 VAL425 ALA427 GLN428 TYR435	VAL256 ARG258 LEU398 LEU424 TYR435	LEU424

Table 4: CB docking for the identification of protein-druggable pockets in the CpsB protein of *S. pneumonia*

Compound	Binding affinity (kcal/mol)	Cavity volume (Å3)	Center (x, y, z)	Docking size (x, y, z)	Contact Residues	Ligand Interactions	H-bond
Gallic acid	-6.2	1515	71, 38, 35	23, 23, 17	HIS136 ASN163 SER164 SER165 HIS166 TYR177 SER198 ASP199 MET200 HIS201 GLY205 ARG206 PRO207 PRO208 HIS209	ASN163 SER165 HIS166 ARG206 PRO207	ASN163 PRO207
6-Gingerol	-5.9	1515	71, 38, 35	24, 24, 24	ASP14 HIS42 GLU80 GLU108 HIS136 GLU138 ARG139 ASN163 SER165 HIS166 TYR177 MET180 SER198 ASP199 HIS201 GLY205 ARG206 PRO207 HIS209	HIS136 SER165 HIS166 TYR177 MET180 ARG206 PRO207	SER165 ARG206
6-Shagaol	-5.9	328	65, 28, 44	24, 24, 24	HIS166 VAL167 LEU168 LYS169 PRO170 LYS178 LYS181 LYS182 ARG183 GLN185 LEU216 GLN219 LYS220 TYR221	PRO170 GLN185 LEU216 LYS220	GLN185
8-Gingerol	-6.4	1515	71, 38, 35	24, 24, 24	HIS42 GLU80 GLU108 HIS136 GLU138 ARG139 ASN163 SER165 HIS166 LYS171 GLY174 GLU175 ARG176 TYR177 MET180 LYS181 SER198 ASP199 HIS201 GLY205 ARG206 PRO207 HIS209	GLU108 HIS136 ARG139 ASN163 SER165 HIS166 LYS171 TYR177 MET180 ASP199 HIS209	GLU108 ASN163 SER165
10-Gingerol	-5.2	1515	71, 38, 35	26, 26, 26	ASP14 HIS42 PHE48 GLU108 HIS136 ARG139 ASN163 SER164 SER165 HIS166 TYR177 MET180 SER198 ASP199 HIS201 GLY205 ARG206 PRO207	ASP14 HIS42 HIS136 SER165 TYR177 MET180 HIS201 GLY205 ARG206	ASP14 SER165 ARG206
Gingerenone A	-6.5	1515	71, 38, 35	21, 21, 21	HIS42 GLU80 GLU108 HIS136 ARG139 ASN163 SER165 HIS166 TYR177 MET180 SER198 ASP199 HIS201 GLY205 ARG206 PRO207	HIS42 HIS136 ASN163 SER165 HIS166 TYR177 SER198 ASP199 HIS201 ARG206	HIS136 ASN163 SER165 SER198
Gingerenone B	-7.3	1515	71, 38, 35	28, 28, 28	HIS42 GLU80 GLU108 HIS136 GLU138 ARG139 ASN163 SER165 HIS166 LEU168 LYS169 LYS171 GLU175 TYR177 MET180 LYS181 SER198 ASP199 HIS201 GLY205 ARG206 HIS209	HIS136 ARG139 ASN163 HIS166 LEU168 LYS171 TYR177 MET180 LYS181 ASP199 ARG206 HIS209	HIS136 ASN163 LYS181
Gingerenone C	-6.4	238	82, 58, 33	24, 24, 24	ARG43 ARG44 LYS45 PHE48 GLU49 THR50 PRO51 GLU52 TYR82 THR84 ASP86 VAL87 LYS90 LYS94 ARG95 ILE9	ARG43 ARG44 LYS45 LYS90 ARG95	
Isogingerenone B	-7.3	1515	71, 38, 35	27, 27, 27	ASP14 HIS42 GLU80 GLU108 HIS136 GLU138 ARG139 ASN163 SER165 HIS166 LYS171 GLY174 GLU175 ARG176 TYR177 MET180 SER198 ASP199 HIS201 GLY205 ARG206 PRO207 HIS209	HIS42 HIS136 ARG139 ASN163 SER165 HIS166 LYS171 GLY174 ARG176 TYR177 MET180 ASP199 ARG206	HIS136 ASN163 SER165 LYS171
Paradol	-5.7	1515	71, 38, 35	24, 24, 24	ASP14 HIS42 GLU108 HIS136 ARG139 ASN163 SER165 HIS166 TYR177 MET180 SER198 ASP199 MET200 HIS201 ARG206 PRO207	HIS136 SER165 HIS166 MET180 SER198 ARG206	SER165 HIS166
Zingerone	-5.7	1515	71, 38, 35	18, 18, 18	HIS42 GLU80 GLU108 HIS136 ARG139 ASN163 SER165 HIS166 TYR177 SER198 ASP199 MET200 HIS201 GLY205 ARG206 PRO207	HIS136 SER165 ARG206 PRO207	HIS136 SER165

Table 5: CB docking for the identification of protein-druggable pockets in the CpsD protein of *S. pneumonia*

Compound	Binding affinity (kcal/mol)	Cavity volume (Å3)	Center (x, y, z)	Docking size (x, y, z)	Contact Residues	Ligand Interactions	H-bond
Gallic acid	-5.6	805	-11, -7, -27	17, 26, 17	ALA7 GLN8 LYS9 LYS10 PHE13 TYR21 GLU47 GLY48 LYS49 THR51 THR52 VAL175 ASN206 LYS207	GLN8 LYS10 TYR21 GLY48 THR51 ASN206 LYS207	GLN8 LYS10 TYR21 GLY48 ASN206 LYS207
6-Gingerol	-5.9	345	-17, 6, -6	24, 24, 24	GLU18 ASN22 CYS25 THR26 ILE28 GLN29 ASP33 LYS34 LEU35 LYS36 SER59 PHE60 ARG62 ALA63 TYR65 TYR148	LEU35 TYR65	TYR65
6-Shagaol	-6.2	345	-17, 6, -6	24, 24, 24	GLU18 ASN22 CYS25 THR26 ILE28 GLN29 GLY32 ASP33 LYS34 LEU35 LYS36 SER59 PHE60 ARG62 ALA63 TYR65 TYR148	CYS25 LEU35 PHE60 ALA63 TYR65	LEU35 TYR65
8-Gingerol	-5.7	345	-17, 6, -6	24, 24, 24	GLU18 ASN22 CYS25 THR26 ILE28 GLN29 GLY32 ASP33 LYS34 LEU35 LYS36 SER59 PHE60 ARG62 ALA63 TYR65 ASP147	GLN29 LEU35 PHE60 TYR65	GLN29 TYR65
10-Gingerol	-5.8	386	-9, -3, 2	26, 26, 26	GLU18 ASN22 CYS25 THR26 ILE28 GLN29 LYS34 LEU35 LYS36 SER59 PHE60 ALA63 TYR65 ASP147 TYR148	CYS25 LEU35 ALA63 TYR65 ASP147	CYS25 LEU35
Gingerenone A	-6.9	345	-17, 6, -6	21, 21, 21	GLU18 ASN22 CYS25 THR26 ILE28 GLN29 ASP33 LYS34 LEU35 LYS36 SER59 PHE60 ARG62 ALA63 TYR65 TYR148	CYS25 LEU35 LYS36 ARG62 ALA63 TYR65	LYS36
Gingerenone B	-6.8	386	-9, -3, 2	28, 28, 28	GLU18 ASN22 CYS25 THR26 ILE28 GLN29 ASP33 LYS34 LEU35 LYS36 SER59 PHE60 ARG62 ALA63 TYR65 ASP147 TYR148	GLU18 CYS25 ILE28 LEU35 LYS36 PHE60 ALA63 TYR65 TYR148	LYS36 TYR65
Gingerenone C	-7	345	-17, 6, -6	24, 24, 24	GLU18 ASN22 CYS25 THR26 ILE28 GLN29 ASP33 LYS34 LEU35 LYS36 SER59 PHE60 ARG62 ALA63 TYR65 ASP147 TYR148	CYS25 LEU35 LYS36 ARG62 ALA63 TYR65	LEU35 TYR65
Isogingerenone B	-6.9	345	-17, 6, -6	27, 27, 27	GLU18 ASN22 CYS25 THR26 ILE28 GLN29 GLY32 ASP33 LYS34 LEU35 LYS36 SER59 PHE60 ARG62 ALA63 TYR65 ASP147 TYR148	GLU18 ASN22 CYS25 LEU35 LYS36 PHE60 ALA63 TYR65	LEU35 TYR65
Paradol	-5.7	345	-17, 6, -6	24, 24, 24	CYS25 ILE28 GLN29 GLY32 ASP33 LYS34 LEU35 LYS36 PHE60 TYR65 ASP147 TYR148	GLN29 ASP33 LYS34 PHE60 TYR65	GLN29
Zingerone	-5.9	345	-17, 6, -6	18, 18, 18	CYS25 ILE28 GLN29 LYS34 LEU35 LYS36 PHE60 TYR65 ASP147 TYR148	LYS34 LYS36 TYR65	LYS36

Table 6: Docking score computed through the MVD approach for the CpsB protein of *S. pneumonia* with compounds of *Zingiber officinale.*

Compounds	MolDock Score (kcal/mol)	Re-Rank Score (kcal/mol)	H-bonds (kcal/mol)	Amino Acids involved in H-bond interaction	H- bonds
10-Gingerol	-119.782	-88.0894	-5.19161	SER165, SER198	2
6-Gingerol	-94.6396	-80.6935	-3.63887	GLU108, SER165	2
6-Shogaol	-112.892	-95.4071	-2.93418	SER165, PRO207	3
8-Gingerol	-121.701	-56.3027	-8.36559	GLU108, HIS136, SER165, ARG206	4
Gingerenone A	-126.534	-90.6231	-7.0358	SER165, HIS201, GLY205, ARG206	4
Gingerenone B	-114.899	-84.4476	-12.9098	ASP14, ASN163, SER165, TYR177, HIS201, GLY205, ARG206, HIS209	8
Gingerenone C	-110.254	-69.9239	-9.28658	ASN163,HIS166,SER165, PRO207	4
Isogingerenone B	-112.262	-74.8476	-4.60206	ASP14, HIS42, SER165 HIS201, ARG206	5
Paradol	-112.34	-89.5699	-3.50943	SER165, HIS166	2
Zingerone	-81.2447	-69.0339	-7.49811	SER165, ARG206,PRO207	3

Table 7: Docking score computed through the MVD approach for the CpsD protein of S. pneumonia with compounds of *Zingiber officinale.*

Compounds	MolDock Score (kcal/mol)	Re-Rank Score (kcal/mol)	H-bonds interaction Energy (kcal/mol)	Amino acids involved in H-Bond interaction	H- bonds
10-Gingerol	-118.74	-45.5627	-8.26115	CYS25, LEU35, LYS36	3
6-Gingerol	-112.106	-75.1628	-3.20513	LEU35, TYR65	2
6-Shogaol	-107.446	-75.4309	-4.15734	LEU35, TYR65	2
8-Gingerol	-106.174	-75.6036	-4.4399	GLN29, GLY32, TYR65	3
Gingerenone A	-121.414	-71.8311	-3.08242	CYST25, ASP33, LYS36	3
Gingerenone B	-126.112	-93.3056	-4.44626	ASN22, LYS36, TYR65	3
Gingerenone C	-120.026	-80.6227	-5.05059	LYS36, TYR65	2
Isogingerenone B	-109.107	-79.297	-4.04508	GLN29, LEU35, LYS36, TYR65	4
Paradol	-112.55	-82.5226	-5.63621	GLN29, GLY32, ASP33, LYS36	4
Zingerone	-75.966	-61.8727	-3.0452	LYS36, TYR65	2

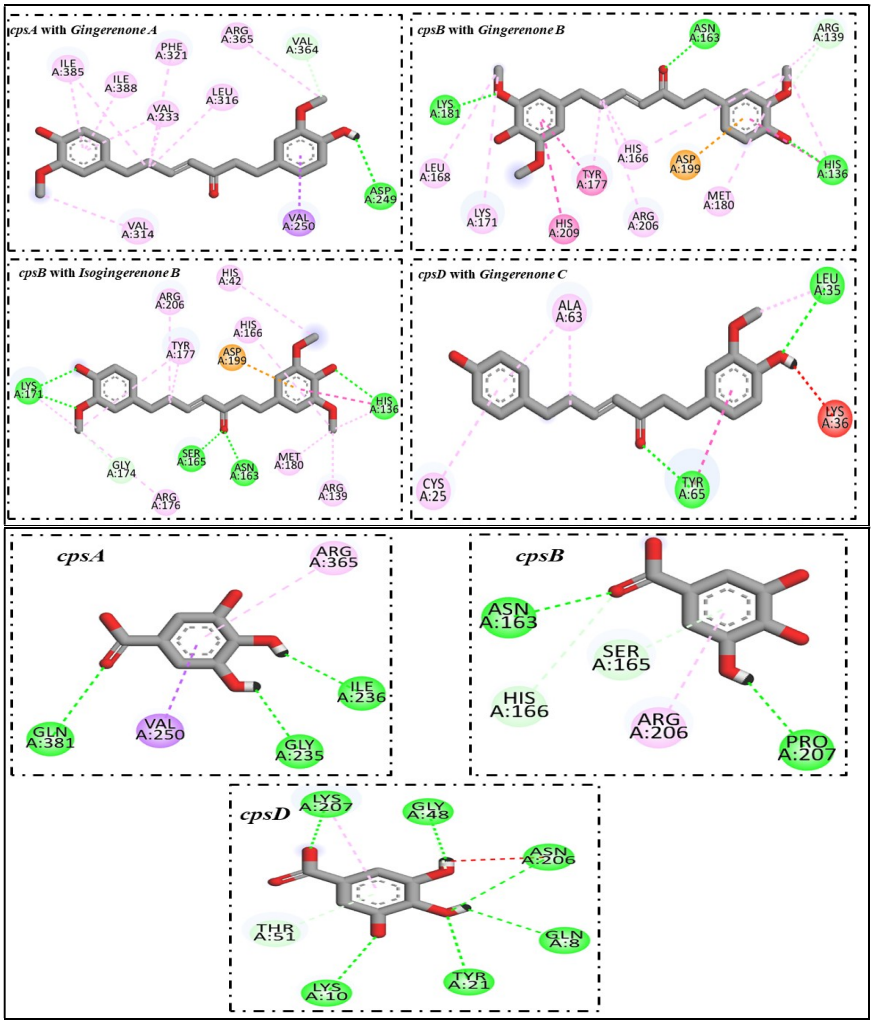

Fig. 1: The first section (lower section) of this diagram shows 2D ligand plots of gallic acid binding (having the highest ΔG values) with CpsA, CpsB, and CpsD proteins of *S. pneumoniae*. The top second section (upper section) of this diagram shows 2D ligand plots of the mentioned bindings of bioactive compounds of *Zingiber officinale* (having the highest ΔG values) with CpsA, CpsB, and CpsD proteins of *S. pneumoniae*. The coloring scheme shows green conventional H-bonds; light green van der Waals; dark purple Pi-Pi stacked; light purple Pi-alkyl; electric blue halogen; light yellow Pi sulfur and light brown Pi-cation or Pi-anion.

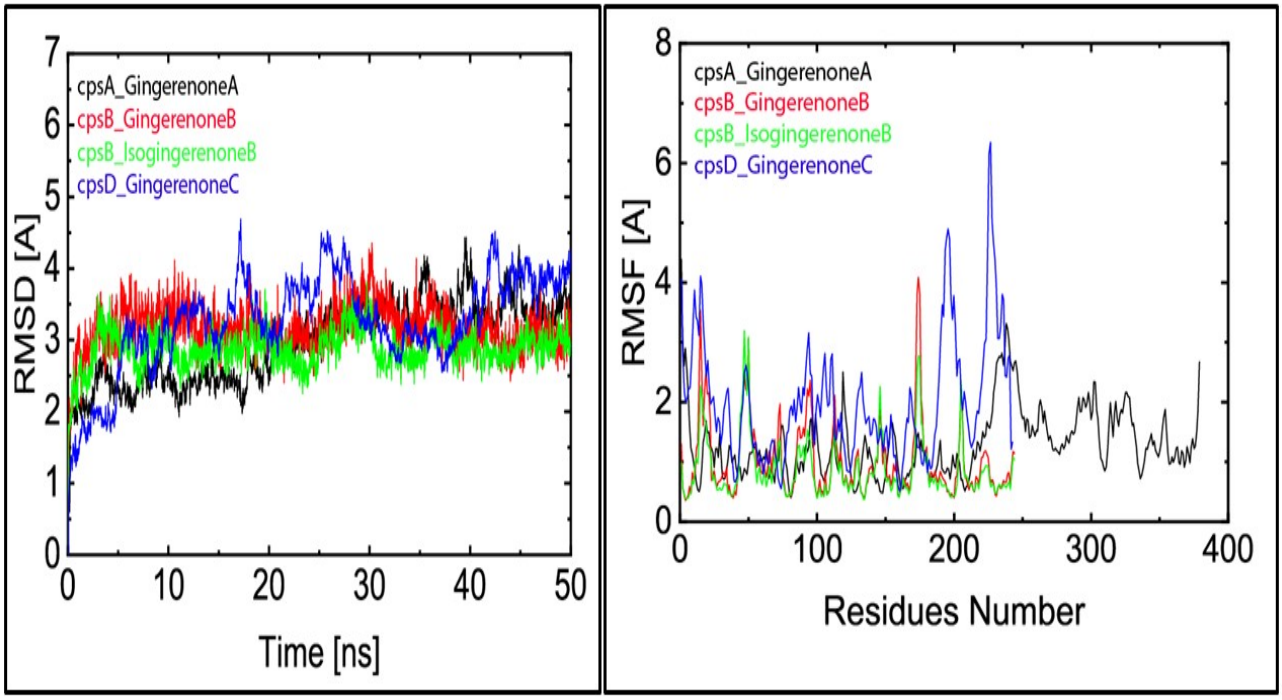

Fig. 2: This figure shows root-mean-square deviation (RMSD) and root-mean-square fluctuation (RMSF) images of all top-ranked compounds of *Zingiber officinale* with the CPS proteins of *S. pneumoniae*. Section 2. A. The black, red, green, and purple graphs show the root main square deviation of CpsA with gingerenone A, CpsB with gingerenone B, CpsB with isogingerenone B, and CpsD with gingerenone C, respectively. Section. 2. B. The RMSF plot of all four complexes has different rates of fluctuation, with red and green having similar trends. This variable fluctuation is due to the different homologous proteins.

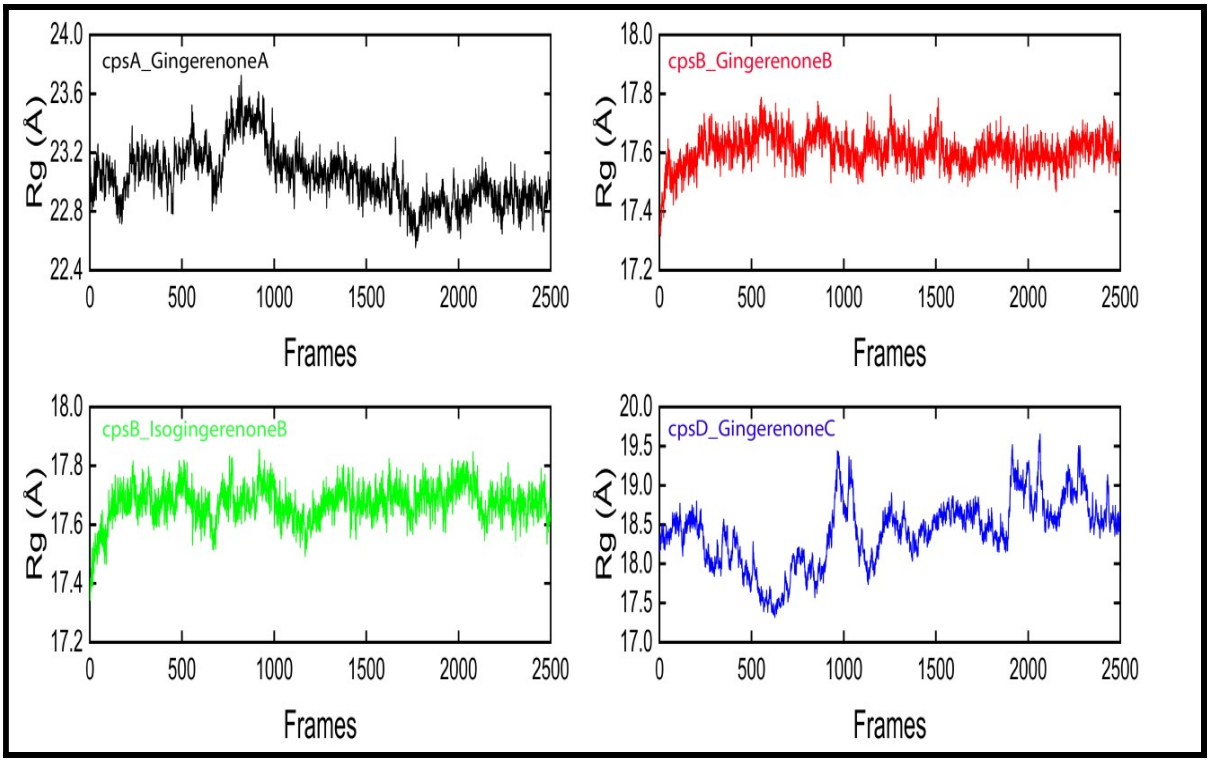

Fig. 3: The radius of gyration (Rg) plot of all four complexes shows a different range and variable behavior.

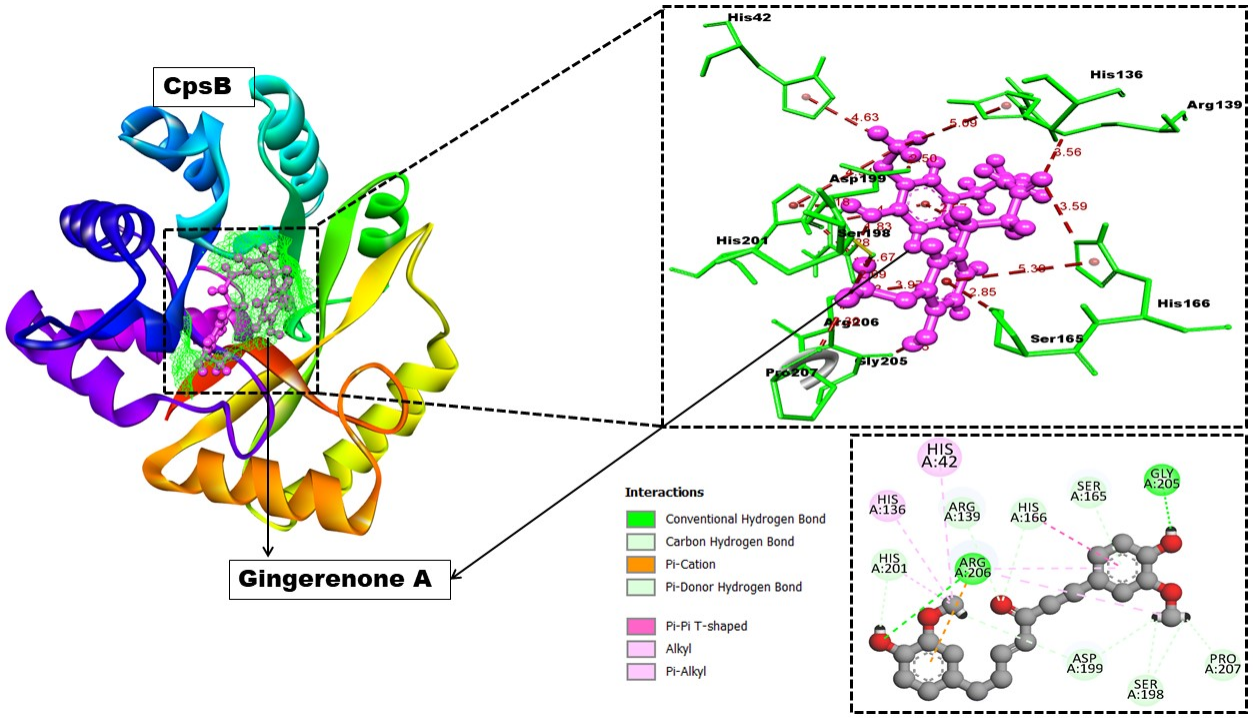

Fig. 4: This figure shows the top-ranked compound molecular interactions of the CpsB protein of *S. pneumonia* with the gingerenone A compound of *Zingiber officinale* determined through the MVD platform. From the figure's interface, the residue's interaction is depicted, and the section below indicates the type of bonding pattern observed during this interaction with the CpsB protein of *S. pneumonia*.

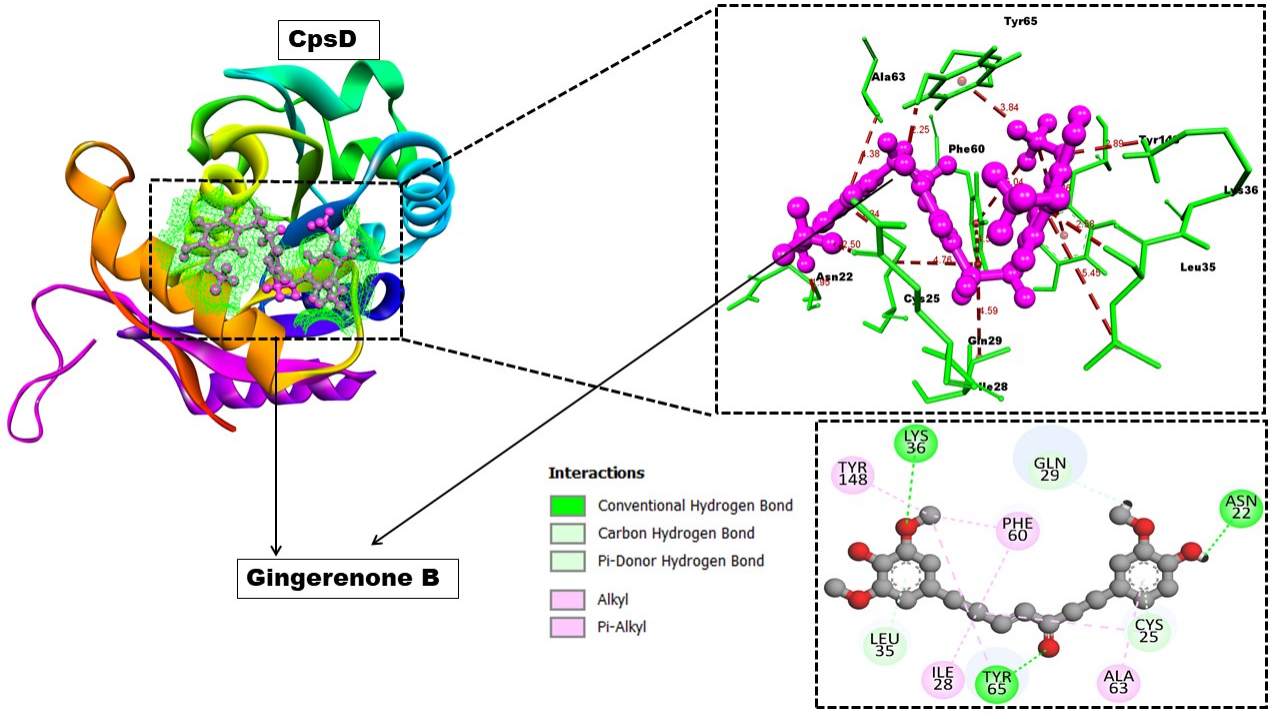

Fig. 5: This figure shows the top-ranked compound molecular interactions of the CpsD protein of *S. pneumonia* with the gingerenone B compound of *Zingiber officinale* determined through the MVD platform. From the figure's interface, the residue's interaction is depicted, and the section below indicates the type of bonding pattern observed during this interaction with the CpsD protein of *S. pneumonia*.

No structural similarity was found in the CpsC protein, which showed no significant structural similarity during the pBLAST PDB database search. Therefore, this protein was excluded from further investigation within the scope of this work. The remaining two homology models, CpsA and CpsD, were built using the MODELLER tool followed by an energy-minimization process (table 2).

Homology modeling of capsular proteins of S. pneumoniae and its structural assessment

The 3D homology models with the lowest MODELLER objective function value, which is the 3D model with the lowest DOPE assessment scores and/or the greatest GA341 assessment score, were considered rational for selecting the top predicted model based on the energetic score estimates. For the CpsA protein of *S. pneumoniae*, initially energy minimization was performed using each obtained model. Subsequently, it was found that among the five obtained consequent homology models, Model 4 had the lowest DOPE score of -45395.32813, lowest molpdf objective function of 2161.97632 and highest GA341 score of 1. Interestingly, this generated an energy-minimized 3D homology model of CpsA from *S. pneumoniae* with the highest quality factor (93.55%). Similarly, for the CpsD protein of *S. pneumoniae*, the same energy minimization process was repeated with each obtained 3D model. Among the five generated 3D models of the CpsD protein of *S. pneumoniae*, it was found that model number 2 had the lowest DOPE score value, i.e., -24296.06641; the molpdf value was 1441.58679; and the GA341 score was 1.00. The generated 3D model had the highest quality factor, that is, >75%.

The 3D stereochemical structural assessment and validation of all selected homology 3D models subjected to further investigation showed satisfactory statistical ranges for the considered parameters. In particular, the obtained quality factors of all three refined 3D models, i.e., CpsA, CpsB and CpsD of *S. pneumoniae*, as well as the availability of the percentage of residues in the most favored regions, were quite satisfactory.

Natural product compounds of Zingiber officinale

The chemical structures of different bioactive compounds from *Zingiber officinale* were downloaded. After the necessary structural transformation and energy minimization, Lipinski's rule of drug-likeness assessment as well as drug property exploration using the OSIRIS tool was performed. A total of ten eligible compounds exhibiting all drug-like properties were found, which were used for further experimentation.

Identification of druggable 3D protein cavities

Because of the lack of active binding site information for selected capsular polysaccharide proteins (i.e., CpsA, CpsB and CpsD) of *S. pneumoniae*, a cavity binding blind docking procedure to obtain the details of consensus binding residues (Liu *et al*., 2020) was adopted. With the CpsA protein, the highest binding affinity was observed with gingerenone A, gingerenone C and gingerenone B, which were -8.8 kcal/mol, -8.7 kcal/mol and -8.6 kcal/mol, respectively (table 3 and fig. 1).

The ligand interaction details of all ten eligible compounds, including the H-bonding pattern with the CpsA protein of *S. pneumoniae*, are shown in table 4 and fig. 1. With the CpsB protein, the CB docking procedure resulted in higher binding affinities with gingerenone B and isogingerenone B as the top-ranked compounds, which were -7.3 kcal/mol. The ligand interaction details of all ten eligible compounds, including the H-bonding pattern with the CpsB protein of *S. pneumonia*, are shown in table 5 and fig. 1. With the CpsD protein, the top-ranked binding affinity compounds were gingerenone C, gingerenone A and isogingerenone B, exhibiting binding energies of -7 kcal/mol and -6.9 kcal/mol, respectively. The ligand interaction details of all ten eligible compounds, including the H-bonding pattern with the CpsD protein of *S. pneumoniae*, are shown in table 6 and fig. 1.

Molecular dynamics (MD) simulation of top-ranked compounds from Zingiber officinale with CPS protein of S. pneumoniae

RMSD calculations were performed for gingerenone A, gingerenone B, isogingerenone B and gingerenone C within the consensus sites of CpsA, CpsB and CpsD, respectively. This was to ensure that all four complexes remained intact over 50 nanoseconds of simulation. The RMSD has an average range of 1.0 Å to 4.5̊ for the system. The RMSD plot of gingerenone A exhibits consistent variations between 2.0 Å and 2.5 Å from 5.0 ns to 20 ns, followed by a stable period up to 30 ns with the same level of deviation for the next 10 ns and finally converged at 3.0 Å for the last 5.0 ns. In contrast, the compounds gingerenone B and isogingerenone B both show similar behaviors, initially an increase in RMSD up to 3.0 Å, followed by a uniform appearance from 10 ns to 30 ns and a stable steady state after 30 ns with an RMSD of 2.5 Å throughout the rest of the simulation. However, the RMSD of gingerenone C increased up to 4.5 Å with some minor declines in the first 20 ns of simulation. This led to perturbations for the next 25 ns, followed by convergence for the next 5.0 ns. Overall, the RMSD in fig. 2 of all four complexes demonstrates that gingerenone B and iso-gingerenone B are tightly bound to the receptor protein, while the RMSD for the remaining two complexes reveals instabilities of these inhibitors in the binding pockets of receptor proteins (fig. 2).

The RMSFs for all ligand complexes were calculated and compared (fig. 3). The RMSF plot for CpsA & CpsB shows an insignificant deviation from its average position,

except for residues after residue 250 in CpsA and 48, 51 and 175 in CpsB. In the CpsD plot, residues 10-20, 200 and 228 moved significantly from their original positions. These fluctuations are far from the active site of proteins and have no direct role in ligand binding. Residue 250 in CpsA is located near the protein's active site, which may affect ligand binding (fig. 2).

Fig. 3 depicts the Rg (radius of gyration) analysis, which reveals that all four complexes have average Rg values in different ranges. The CpsB in both complexes exhibit a similar gyration trend and demonstrate high compactness when the ligand is bound, as evidenced by stabilization in the last 1100 frames of the MD simulation. However, the Rg plot for CpsA and CpsD showed a more oscillating pattern and the impact of ligand binding on protein structure compactness. The Rg profiles for all complexes demonstrate that CpsB in both complexes (red & green) has a stable compact structure with average values of 17.4-17.8, whereas CpsA and CpsB (black and blue) appear to have deviated significantly from their center of mass throughout the simulation. Our results show that gingerenone B and iso-gingerenone B formed strong interactions with the proteins, while gingerenone A and gingerenone C showed more movement. The protein parts near the binding sites remained relatively stable, but some areas farther away moved further. The proteins in the complexes with gingerenone B remained compact, while those with gingerenone A and gingerenone C had more structural changes.

Re-docking approach through MVD (Molegro Virtual Docker) tool for CpsB and CpsD protein of Streptococcus pneumonia with compounds of Zingiber officinale

With the aid of the MVD docking tool, the CpsB and CpsD proteins of *S. pneumoniae* were analyzed with compounds of *Zingiber officinale* in terms of their inhibition potential. In particular, their re-rank and H-bond formation energies support their inhibitory potential for the Cps protein of *S. pneumoniae* (table 6-7 and fig. 5-6). The pattern and computation of the number of H-bonds formed also support the present objective. MVD was used for the validation of the CpsB and CpsD proteins of *S. pneumoniae* with compounds of *Zingiber officinale* in terms of their inhibition potential (tables 6-7 and fig. 4-5). The pattern and computation of the number of H-bonds formed also supported the previously generated data.

DISCUSSION

Antibiotic resistance is a global concern, particularly in *S. pneumoniae*, a gram-positive bacterium responsible for millions of deaths (Jayaraman *et al.,* 2019; Subramanian *et al.,* 2019). The capsule, a key virulence factor, is lost, leading to weakening or complete virulence (Geno *et al.,* 2015; Gonzales-Siles *et al.,* 2019). The study aimed to investigate the inhibitory potential of active ginger compounds against capsule-synthesizing proteins from *S. pneumoniae*.

Bacteria's virulence is often attributed to their capsular polysaccharide (CPS) structure, which plays a crucial role in immune evasion and pathogenicity (Paton and Trappetti, 2019; Gonzales-Siles *et al.,* 2019). The diversity in capsular polysaccharides contributes to bacterial evasion and disease (Skov Sørensen *et al.,* 2016; Gonzales-Siles *et al*., 2019). This study focuses on selecting conserved capsular protein targets to generalize findings and design inhibitors to manage infections associated with *S. pneumoniae*. Research shows that CPS proteins prevent immune cell phagocytosis, inhibit complement-mediated lysis and mask bacterium surface antigens, making it difficult for the immune system to recognize and eliminate bacteria (Lane *et al.,* 2022; Paton and Trappetti, 2019). To investigate these proteins, 3D protein homology models were created using homology modeling, a computational technique in structural biology. MODELLER was chosen for its user-friendly interface, reliability and effectiveness in producing accurate homology models (Webb and Sali, 2021). Homology modeling plays a significant role in bioinformatics, providing insights into 3D structures of biomolecules (Hameduh *et al.,* 2020). The CpsA and CpsD protein sequences were modeled using an algorithm-based approach, with the best model chosen based on the lowest objective function value.

Zingiber officinale has significant phytomedicinal importance because of its diverse array of bioactive compounds, such as gingerol, shogaol and zingerone (Zhang *et al.,* 2021). Generally, the diverse pharmacological activities of *ginger* compounds make them valuable substances in the drug discovery process. Therefore, in the absence of prominent active site information in selected proteins of *S. pneumoniae*, the focus was on identifying druggable protein cavities using the bioactive medicinal compounds of *Zingiber officinale*. The CB docking interactions of conserved CPS proteins showed significant binding affinity with a large number of bioactive compounds from *Zingiber officinale*. Keeping this in mind, the identification of druggable cavities in above conserved CPS proteins can lead to the repurposing of existing drugs for new therapeutic indications. Moreover, the screened compounds from *Zingiber officinale* are known to interact with particular cavities of conserved CPS proteins; hence, they may be investigated for their potential efficacy against different diseases. Relating these outcomes with previously reported antimicrobial properties of ginger extends to both gram-positive and gram-negative bacteria, making it a promising candidate for combating bacterial infections (Oyinlola *et al.,* 2022). Additionally, its activity against

fungal pathogens underscores its potential in addressing fungal overgrowth issues. The multifaceted antimicrobial effects of *Zingiber officinale* contribute to its role as a valuable natural resource in promoting health and wellness, although further research is required to fully elucidate its therapeutic applications (Zhang *et al.,* 2021).

MD simulations offer crucial insights into the dynamic behavior of biomolecules, revealing their movement, interactions and conformational changes, which are essential for understanding biological functions and reaction pathways (Guterres and Im, 2020). Using the MD simulation experimentation strategy, the stability of four compounds (gingerenone A, gingerenone B, isogingerenone B and gingerenone C) was examined when they interacted with CpsA, CpsB and CpsD to determine whether these interactions remained strong during a 50-nanosecond simulation. To gain insight into protein backbone flexibility, MD trajectories were used to calculate the root mean square fluctuations for all complexes. During thermal motion and solvent interactions, some protein residues may undergo considerable distortion from their average structure. The smaller the RMSF value, the fewer residues fluctuate, whereas when it is higher, the residues move more from their initial states. MD simulations in bioinformatics analysis bridge the gap between static experimental structures and the dynamic nature of biomolecules, offering a wealth of information regarding their behavior and interactions (Hollingsworth and Dror, 2018). Interestingly, among the four complexes, the interaction of CpsB with gingerenone B and isogingerenone B compound complexes had a significantly stable RMSD curve. The outcomes from the RMSF computation of the top-ranked complexes, CpsB with gingerenoneB and isogingerenoneB showed prominent compactness. This means that these two complexes adopt some conformational changes by binding to the concerned ligand, as discussed above. Similarly, the Rg (radius of gyration) was measured to assess the tightness and entropy of folding in the secondary structures of the receptor protein upon binding to a ligand. A higher Rg value indicates a loss of compactness, whereas a lower value indicates tighter confirmation of the protein structure. MD simulations assist in rational drug design by simulating the interactions between drug candidates and target proteins, guiding the design of compounds with optimal binding properties and minimizing off-target effects (Guterres and Im, 2020; Hollingsworth and Dror, 2018).

Further to this, our results were validated using Molegro Virtual Docker (MVD), a computational tool designed for molecular docking. MVD is used to explore various ligand-binding poses and predict their binding affinities, which helps in identifying potential drug candidates (Bitencourt-Ferreira and de Azevedo, 2019). This experimental protocol investigated the potential for inhibition of compounds from *Zingiber officinale* against the CpsB and CpsD proteins of *S. pneumoniae* using the MVD docking program. The calculation of the number of H-bond formations and their pattern both support the current goal using the MVD platform. This strategy further ensures the validity of our findings for the future use and selection of these compounds for the inhibition of CPS in *S. pneumoniae*.

CONCLUSION

The study reveals that ginger bioactive compounds can inhibit the capsular biosynthesis genes of *S. pneumoniae*, indicating potential therapeutic applications. Further research is needed to confirm these findings, investigate bioavailability, toxicity and off-target effects. In addition, their activity against other capsular bacteria, such as *Klebsiella* and *Staphylococcus aureus*, can also be studied.

ACKNOWLEDGMENT

The authors would like to extend their sincere appreciation to the Researchers Supporting Project Number (RSP2024R301), King Saud University, Riyadh, Saudi Arabia.

REFERENCES

Aliberti S, Cook G S, Babu BL, Reyes LF, Rodriguez AH, Sanz F, Soni NJ, Anzueto A, Faverio P, Sadud RF, Muhammad I, Prat C, Vendrell E, Neves J, Kaimakamis E, Feneley A, Swarnakar R, Franzetti F, Carugati M, Morosi M, Monge E and Restrepo MI (2019). International prevalence and risk factors evaluation for drug-resistant *Streptococcus pneumoniae* pneumonia. *J. Infect.* **79**(4): 300-311.

AlSheikh HMA, Sultan I, Kumar V, Rather IA, Al-Sheikh H, Tasleem Jan A and Haq QMR (2020). Plant-based phytochemicals as possible alternative to antibiotics in combating bacterial drug resistance. *Antibiotics* **9**(8): 480-503.

Bitencourt-Ferreira G and de Azevedo WF (2019). Molegro virtual docker for docking, *In*: De Azevedo WF (Ed.). Docking screens for drug discovery. *Methods Mol. Biol.,* **2053**: 149-167.

Chen X, Li H, Tian L, Li Q, Luo J and Zhang Y (2020). Analysis of the physicochemical properties of acaricides based on Lipinski's rule of five. *J. Comput. Biol.,* **27**(9): 1397-1406.

Croucher NJ, Chewapreecha C, Hanage WP, Harris SR, McGee L, van der Linden M, Song JH, Ko KS, de Lencastre H, Turner C, Yang F, Sá-Leão R, Beall B, Klugman KP, Parkhill J, Turner P and Bentley SD (2014). Evidence for soft selective sweeps in the evolution of pneumococcal multidrug resistance and vaccine escape. *Genome Biol. Evol.,* **6**(7): 1589-1602.

Dallakyan S and Olson AJ (2015). Small-molecule library screening by docking with PyRx. *In*: Hempel JE, Williams CH and Hong CC (Eds.), Chemical biology. *Methods Mol. Biol.,* **1263**: 243-250.

Elmaidomy AH, Shady NH, Abdeljawad KM, Elzamkan MB, Helmy HH, Tarshan EA, Adly AN, Hussien YH, Sayed NG, Zayed A and Abdelmohsen UR (2022). Antimicrobial potentials of natural products against multidrug resistance pathogens: A comprehensive review. *RSC Adv.* **12**(45): 29078-29102.

Gao YD and Huang JF (2011). An extension strategy of Discovery Studio 2.0 for non-bonded interaction energy automatic calculation at the residue level. *Dongwuxue Yanjiu.* **32**(3): 262-266

Geno KA, Gilbert GL, Song JY, Skovsted IC, Klugman KP, Jones C, Konradsen HB and Nahm MH (2015). Pneumococcal capsules and their types: Past, present and future. *Clin. Microbiol. Rev.* **28**(3): 871-899.

Goodsell DS, Zardecki C, Di Costanzo L, Duarte JM, Hudson BP, Persikova I, Segura J, Shao C, Voigt M, Westbrook JD, Young JY and Burley SK (2020). RCSB protein data bank: Enabling biomedical research and drug discovery. *Protein Sci.,* **29**(1): 52-65.

Gonzales-Siles L, Salvà-Serra F, Degerman A, Nordén R, Lindh M, Skovbjerg S and Moore ERB (2019). Identification and capsular serotype sequetyping of Streptococcus pneumoniae strains. *J. Med. Microbiol.,* **68**(8): 1173-1188.

Guex N, Peitsch MC and Schwede T (2009). Automated comparative protein structure modeling with SWISS-MODEL and Swiss-PdbViewer: A historical perspective. *Electrophoresis,* **30**(1): S162-S173.

Guterres H and Im W (2020). Improving protein-ligand docking results with high-throughput molecular dynamics simulations. *J. Chem. Inf. Model.,* **60**(4): 2189-2198.

Hameduh T, Haddad Y, Adam V and Heger Z (2020). Homology modeling in the time of collective and artificial intelligence. *Comput. Struct. Biotechnol. J.* **18**: 3494-3506.

Hollingsworth SA and Dror RO (2018). Molecular dynamics simulation for all. *Neuron* **99**(6): 1129-1143.

Jayaraman R, Varghese R, Kumar JL, Neeravi A, Shanmugasundaram D, Ralph R, Thomas K and Veeraraghavan B (2019). Invasive pneumococcal disease in Indian adults: 11 years' experience. *J. Microbiol. Immunol. Infect.,* **52**(5): 736-742.

Kim S, Chen J, Cheng T, Gindulyte A, He J, He S, Li Q, Shoemaker BA, Thiessen PA, Yu B, Zaslavsky L, Zhang J and Bolton EE (2019). PubChem 2019 update: improved access to chemical data. *Nucleic Acids Res.,* **47**(D1): D1102-D1109.

Lane JR, Tata M, Briles DE and Orihuela CJ (2022). A jack of all trades: The role of pneumococcal surface protein a in the pathogenesis of streptococcus pneumoniae. *Front. Cell. Infect. Microbiol.* **12**: 826264.

Lin TH, Wu CC, Tseng CY, Fang JH and Lin CT (2022). Effects of gallic acid on capsular polysaccharide biosynthesis in *Klebsiella pneumoniae*. *J. Microbiol. Immunol. Infect.* **55**(6): 1255-1262.

Liu Y, Grimm M, Dai W, Hou M, Xiao ZX and Cao Y (2020). CB-Dock: a web server for cavity detection-guided protein-ligand blind docking. *Acta Pharmacol. Sin.,* **41**(1): 138-144.

Liu Y, Yang X, Gan J, Chen S, Xiao ZX and Cao Y (2022). CB-Dock2: Improved protein-ligand blind docking by integrating cavity detection, docking and homologous template fitting. *Nucleic Acids Res.,* **50**(W1): W159-W164.

Mao QQ, Xu XY, Cao SY, Gan RY, Corke H, Beta T and Li HB (2019). Bioactive compounds and bioactivities of ginger (*Zingiber officinale* Roscoe). *Foods,* **8**(6): 185.

Nguyen NT, Nguyen TH, Pham TNH, Huy NT, Bay MV, Pham MQ, Nam PC, Vu VV and Ngo ST (2020). Autodock vina adopts more accurate binding poses but autodock4 forms better binding affinity. *J. Chem. Inf. Model.,* **60**(1): 204-211.

Olarte L and Jackson MA (2021). *Streptococcus pneumoniae*. *Pediatr. Rev*., **42**(7): 349-359.

Oligbu G, Fry NK and Ladhani SN (2019). The pneumococcus and its critical role in public health. *In*: Iovino, F. (Ed.), Streptococcus Pneumoniae, *Methods Mol. Biol*., **1968**: 205-213.

Oriola AO and Oyedeji AO (2022). Plant-derived natural products as lead agents against common respiratory diseases. *Molecules,* **27**(10): 3054.

Oyinlola KA, Ogunleye GE, Akintade OO, Adeyemo OM and Garuba EO (2022). Bioactive compound profiling and *in-vitro* antimicrobial study of ginger (*Zingiber officinale* Roscoe) extract against pneumococcal bacteria. *Turk. J. Agric. - Food Sci. Technol.* **10**(2): 2920-2925.

Ozkur M, Benlier N, Takan I, Vasileiou C, Georgakilas AG, Pavlopoulou A, Cetin Z and Saygili EI (2022). Ginger for healthy ageing: A systematic review on current evidence of its antioxidant, anti-Inflammatory and anticancer properties. *Oxid. Med. Cell. Longev*., **4748447**: 1-16.

Paton JC and Trappetti C (2019). *Streptococcus pneumoniae* capsular polysaccharide. *Microbiol. Spectr.,* **7**(2): 1-15.

Pettersen EF, Goddard TD, Huang CC, Meng EC, Couch GS, Croll TI, Morris JH and Ferrin TE (2021). UCSF CHIMERAX: Structure visualization for researchers, educators and developers. *Protein Sci.,* **30**(1): 70-82.

Pletz MW, Maus U, Krug N, Welte T and Lode H (2008). Pneumococcal vaccines: mechanism of action, impact on epidemiology and adaption of the species. *Int. J. Antimicrob. Agents,* **32**(3): 199-206.

Rangwala SH, Kuznetsov A, Ananiev V, Asztalos A, Borodin E, Evgeniev V, Joukov V, Lotov V, Pannu R, Rudnev D, Shkeda A, Weitz EM and Schneider VA

(2021). Accessing NCBI data using the NCBI sequence viewer and genome data viewer (GDV). *Genome Res.,* **31**(1): 159-169.

Salomon-Ferrer R, Case DA and Walker RC (2013). An overview of the Amber biomolecular simulation package: Amber biomolecular simulation package. *Wiley Interdiscip. Rev. Comput. Mol. Sci.,* **3**(2): 198-210.

Shah N, Nute MG, Warnow T and Pop M (2019). Misunderstood parameter of NCBI BLAST impacts the correctness of bioinformatics workflows. *Bioinformatics,* **35**(9): 1613-1614.

Skov Sørensen UB, Yao K, Yang Y, Tettelin H and Kilian M (2016). Capsular polysaccharide expression in commensal *Streptococcus* species: Genetic and antigenic similarities to *Streptococcus pneumoniae*. *mBio,* **7**(6): e01844-16.

Subramanian K, Henriques-Normark B and Normark S (2019). Emerging concepts in the pathogenesis of the *Streptococcus pneumoniae* : From nasopharyngeal colonizer to intracellular pathogen. *Cell. Microbiol.,* **21**(11): e13077.

Timalsina D, Pokhrel KP and Bhusal D (2021). Pharmacologic activities of plant-derived natural products on respiratory diseases and inflammations. *BioMed Res. Int.,* **2021**: 1636816.

Wadood A, Shareef A, Ur Rehman A, Muhammad S, Khurshid B, Khan RS, Shams S and Afridi SG (2022). *In silico* drug designing for ala438 deleted ribosomal protein S1 (RpsA) on the basis of the active compound *Zrl* 15. *ACS Omega,* **7**(1): 397-408.

Wang Y, Wang Q, Huang H, Huang W, Chen Y, McGarvey PB, Wu CH, Arighi C.N and on behalf of the UniProt Consortium (2021). A crowdsourcing open platform for literature curation in UniProt. *PLOS Biol.,* **19**(12): e3001464.

Webb B and Sali A (2021). Protein structure modeling with MODELLER. *In*: Chen YW, Yiu CPB (Eds.), Structural genomics. *Methods Mol. Biol.,* **2199**: 239-255.

Yoshikawa N and Hutchison GR (2019). Fast, efficient fragment-based coordinate generation for Open Babel. *J. Cheminformatics,* **11**(1): 49.

Zhang M, Zhao R, Wang D, Wang L, Zhang Q, Wei S, Lu F, Peng W and Wu C (2021). Ginger (*Zingiber officinale* Rosc.) and its bioactive components are potential resources for health beneficial agents. *Phytother. Res.,* **35**(2): 711-742.